Tropospheric and Stratospheric Temperature Profiling with Rotational Raman Lidar:
Design of a Highly Efficient Receiver and Measurement Results

Andreas Behrendt, Jens Reichardt, Claus Weitkamp
Institut für Physikalische und Chemische Analytik,
GKSS-Forschungszentrum GmbH, Postfach 1160, D-21494 Geesthacht, Germany
Tel: +49 4152 87 1828, Fax: +49 4152 871888, E-mail: andreas.behrendt@gkss.de

1 Introduction

A highly efficient rotational Raman lidar receiver for atmospheric nighttime temperature profiling was developed as part of the GKSS Raman lidar (Behrendt et al., 1998; Behrendt and Reichardt, 1999), a mobile container-based system for aerosol parameter, ozone and moisture measurements (Reichardt et al., 1996; Weitkamp et al. 1999). The rotational Raman technique was chosen because it is the only lidar technique so far for the measurement of tropospheric and stratospheric temperature profiles that is not perturbed by the presence of aerosols or cloud particles. The setup utilizes multi-cavity interference filters mounted sequentially with small angles of incidence. Main advantages of this design are high signal throughput, high out-of-band blocking and spectral adjustability of the filter center wavelengths, combined with a stable and relatively simple experimental setup. No systematic error due to residual elastically backscattered light in the rotational Raman channels was observed in clouds up to a backscatter ratio of 45. Temperature height profiles have been measured up to more than 40 km height. Minimum integration time for a statistical temperature error of ±1 K at 960 m resolution is ~5 minutes in the tropopause region and 1.5 hours at 20 km height. Hence, high-resolution lidar studies of, e.g., cloud formation processes become feasible. In this contribution, the polychromator design is outlined and measurement examples are presented.

2 Rotational Raman technique

The rotational Raman technique is the only technique that allows, in theory, the measurement of atmospheric temperature profiles remotely by lidar even in the presence of clouds or aerosol particles (Arshinov et al., 1983; Nedeljkovic et al., 1993; Vaughan et al., 1993). This is in contrast to the widely applied Rayleigh integration method which yields excellent results above the stratospheric aerosol layer, but fails in and below regions of high particle burden. The attempt to reduce the particle influence by use of the molecular-nitrogen vibrational-rotational Raman signal instead of the elastic signal was successful if the Mie contribution remained below 10 % of the Rayleigh backscattering (Keckhut et al., 1990). Otherwise the error due to particle extinction became unacceptable.

But even for the rotational Raman technique, sufficient suppression of the elastic backscattering in the rotational Raman return signals is a challenging topic. With the presented system, lidar temperature measurements in clouds were carried out for the first time to the authors' best knowledge.

The rotational Raman method suggested by Cooney (1972) is based on different temperature derivatives of the intensities of low- and high-quantum-number transitions of the pure rotational Raman spectrum (PRRS). While the intensity of PRRS lines at wavelengths near the exciting laser line decreases with increasing temperature, the intensity of lines with greater wavelength difference increases. By detecting signals in two spectral regions of different temperature dependence and calculating the ratio of the signal intensities, a normalized parameter is derived that, after calibration of the instrument with a radiosonde, yields the atmospheric temperature.

In simulations we found the optimum central wavelengths (CWL) and transmission widths of the rotational Raman channel filters, i.e., the filter data that yield the smallest statistical error in the temperature range of interest (Behrendt and Reichardt, 1999). The PRRS of N_2 and O_2 were calculated separately and superimposed considering the atmospheric volume mixing ratios of 0.781 and 0.209, respectively. In order to avoid the risk of interference of the Stokes branch with fluorescence (Kitada et al., 1994), we decided to extract parts of only the anti-Stokes branch of the PRRS. For the calculations the linear calibration function $R(T)=\alpha T+\beta$ was applied to simulated backscatter data between $T = 185$ and 190 K, the condensation temperatures of polar stratospheric clouds. Here, $R = n_h / n_l$ is the ratio of the number of photons n_h and n_l calculated for the high- and low-quantum-number rotational Raman channels, respectively, T is the temperature, and α, β are fit coefficients.

As primary radiation the emission of a Nd:YAG laser at the wavelength λ_0 = 532.25 nm with a pulse energy of 200 mJ at 50 Hz repetition rate is used. For a full width of 0.55 and 1.2 nm for the low- and high-quantum-number rotational Raman channel filter, optimum CWLs are 531.70 and 529.35 nm, respectively. The values for the filter transmission widths were chosen in an iterative process. Filter parameters that promised sufficient blocking at the laser wavelength were found in cooperation with the manufacturer of the filters, Barr Associates Inc., Westford, MA, USA.

3 Receiver setup

In the first step the spectral separation of atmospheric backscatter light is carried out with a device installed above the primary focus of the receiving telescope which has a diameter of 0.9 m. The elastic and Raman signals of each of the three primary wavelengths of the GKSS Raman lidar are coupled into separate optical fibers, with an additional separation of the two polarizations for the return signal to the 354.85-nm emission. Two separate polychromators are used, one for the signals in the ultraviolet and the one which is described here for those in the visible (Fig. 1).

Light with wavelengths $\geq$ 500 nm is transmitted from the preselection unit to the rotational Raman temperature polychromator. After collimation by lens L1 the incoming light is cascaded down from one detection channel to the next. Almost no losses of signal power occur in the spectral separation process with multi-cavity interference filters mounted sequentially under small angles of incidence.

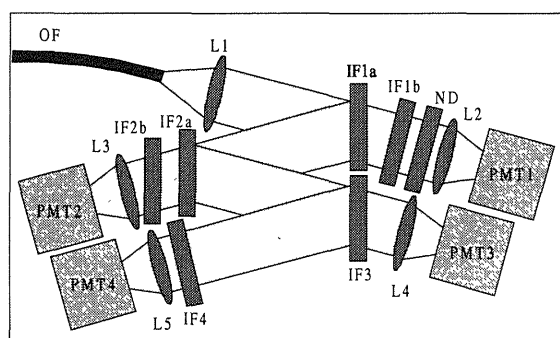First, the 532.25-nm elastic backscattering is separated. The rotational Raman wings are reflected

Figure 1. Setup of the polychromator: OF, optical fiber; L1 to L5, lenses; IF1a to IF4, interference filters; ND, neutral density attenuator; PMT1 to PMT4, photomultiplier tubes for the detection of the elastic, low- and high-quantum-number rotational Raman, and N_2 vibrational-rotational Raman signals, respectively.

nearly totally from IF1a while the elastically backscattered light is attenuated in reflection by one order of magnitude; IF1b is used for further attenuation of the ultraviolet lidar primary signals. IF2a and IF2b filter off low- and IF3 high-quantum-number rotational Raman light. The last detection channel is for the N_2 vibrational-rotational Raman signal centered at 607.63 nm. For the high-quantum-number PRRS channel a single interference filter is employed, yet for the low-quantum-number PRRS channel two filters in line are needed for sufficient blocking of the excitation wavelength λ_0. The receiver optical thickness at λ_0 is ≥ 7 for both PRRS channels. As the thermal drift of the CWL is only 0.002 nm/K no temperature stabilization of the polychromator is needed.

The filters were designed for angles of incidence of φ = 5°. The CWL $\lambda(\varphi)$ can be tuned to both shorter and longer wavelengths by selecting φ. The polychromator was finally aligned by tuning the filters to settings in which no elastic-backscattering enhancement in cloudy regions was observed in the PRRS channels; in this process IF2a and IF2b had to be tilted from φ = 5° to φ = 7°. With this setting, observations show no degradation of the accuracy of the temperature determination even in tropospheric clouds. The final system parameters are given in Table 1.

Table 1. Parameters of the used interference filters in final alignment: AOI, angle of incidence; CWL, center wavelength; FWHM, full width at half maximum; τ, transmittance; ρ, reflectivity.

Wavelength, nm	Parameter	IF1a	IF2a,b comb.	IF3
	AOI, deg.	5.0	7.0	5.0
	CWL, nm	532.40	530.85	529.35
	FWHM, nm	0.74	0.55	1.20
532.25	τ	0.83	$< 10^{-6}$	$< 10^{-6}$
	ρ	0.11		
530.85	τ		0.40	$< 2 \cdot 10^{-4}$
	ρ	> 0.95		
529.35	τ			0.70
	ρ	> 0.96	> 0.96	
608	τ			
	ρ	> 0.96	> 0.96	> 0.96
308	τ	0.08	$< 10^{-10}$	$< 10^{-6}$
355	τ	0.50	$< 10^{-10}$	$< 10^{-6}$

4 Receiver performance

It is interesting to note that with the actual filter setup the polychromator is close to the theoretical optimum.

With future more sophisticated filters than the currently available ones which allow the use of even more temperature-sensitive lines of the PRRS, the statistical error of a temperature measurement could be decreased by only another 26 %, for the same signal power and FWHM.

The tunability of the filter CWLs is not only advantageous for maximizing the suppression of elastic light in the PRRS channels, but also allows the experimentalist to optimize the polychromator sensibility for temperature measurements in different atmospheric temperature ranges or to increase the temperature sensibility at the expense of systematic temperature errors in cloudy regions. A possible long-term drift of the interference filter CWLs by aging which may be caused by humidity uptake could be corrected for, too.

The described temperature polychromator is stable. At least for a period of several days the lidar calibration function remains unchanged within its statistical uncertainty. The minimum measurement integration times for given 1-σ temperature errors needed with the GKSS Raman lidar are shown in Fig. 2 as a function of height. A gliding average of 960 m length was applied for the calculations to 1 hour of best lidar data. Under optimum clear sky conditions a temperature measurement with an error of $\pm$ 1 K at 20 km height takes ~1.5 hours, and dynamical processes in the tropopause region can be observed with a temporal resolution of a few minutes.

5 Measurement examples

First atmospheric measurements with the rotational Raman receiver were made in January and February

Figure 2. Minimum GKSS-Raman-lidar integra-tion time necessary to achieve a statistical 1-σ uncertainty of $\pm$1, $\pm$2, $\pm$5, and $\pm$10 K. For the calculation, 1 hour of best lidar data were taken and smoothed with a 960-m gliding average window.

1998 at the Swedish research facility Esrange (67.9 °N, 21.1 °E) near Kiruna (Behrendt et al., 1999). As an example for measurements in the troposphere, temperature profiles from 28 January, 1998, are shown in Fig. 3. The instrument was calibrated with a local radiosonde started at the beginning of the measurement. Consecutively taken data with 10 minutes integration time were smoothed with 960 m gliding average window length. At this resolution the 1-σ statistical temperature error is in this case about $\pm$1 K in 10 km height. The variation of the tropopause height between 7.5 and 9 km as well as a wavelike pattern in the lower stratosphere can be seen.
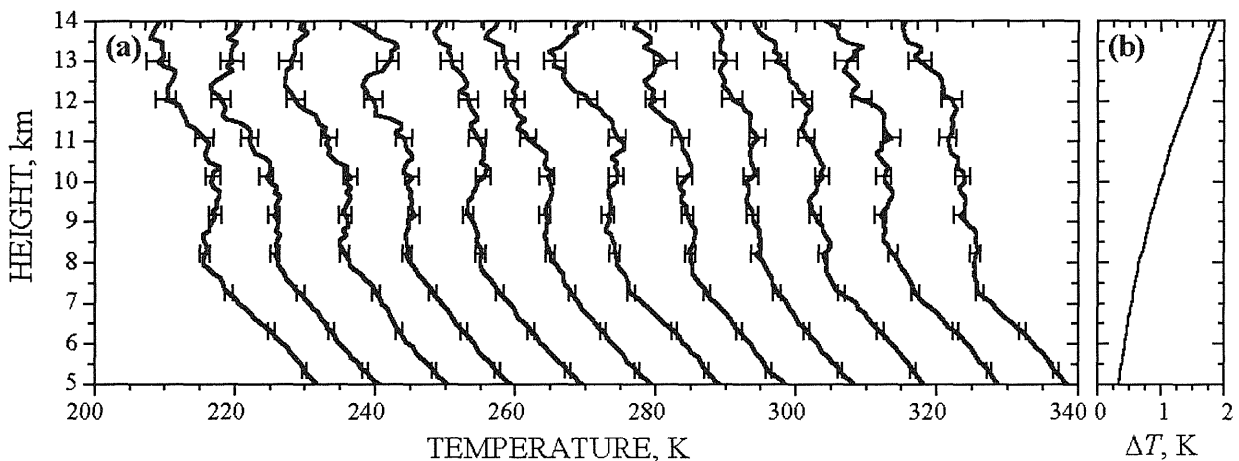

Figure 3. Tropospheric temperature profiling with rotational Raman lidar: measurements at Esrange (67.9 °N, 21.1 °E) on 28 January 1998 beween 15:20 and 17:20 UT. (a) Consecutively taken data with 10 minutes integration time are shown with 10 K offset between two profiles. A 960-m gliding average window was applied. Error bars indicate 1-σ statistical errors. (b) 1-σ statistical temperature error of the last profile against height.
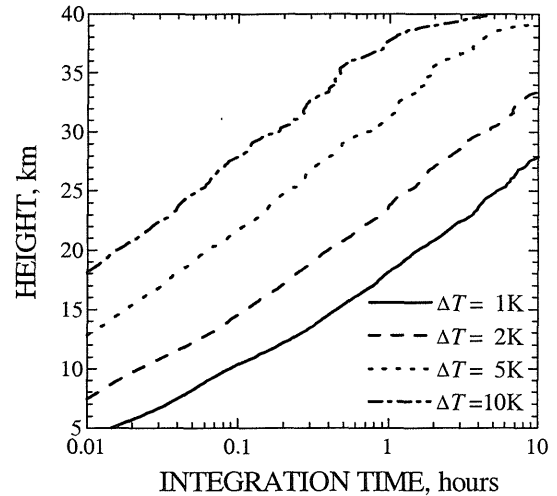
Fig. 4 shows examples of stratospheric temperature measurements taken at Esrange on 24 January 1998. Profiles of about 45 minutes integration time taken in the presence of polar stratospheric clouds (PSCs) are shown together with a 5-hour mean. The strong gravity wave structure on the profiles with minima in coincidence with higher values of the backscatter ratio reveals that the observed PSCs are induced by mountain waves of the Scandinavian mountain ridge.

6 Conclusion

A lidar receiver for temperature measurements with the rotational Raman technique was developed. The instrument employs interference filters mounted sequentially with small angles of incidence. It is highly efficient, spectrally adjustable, easy to handle, and
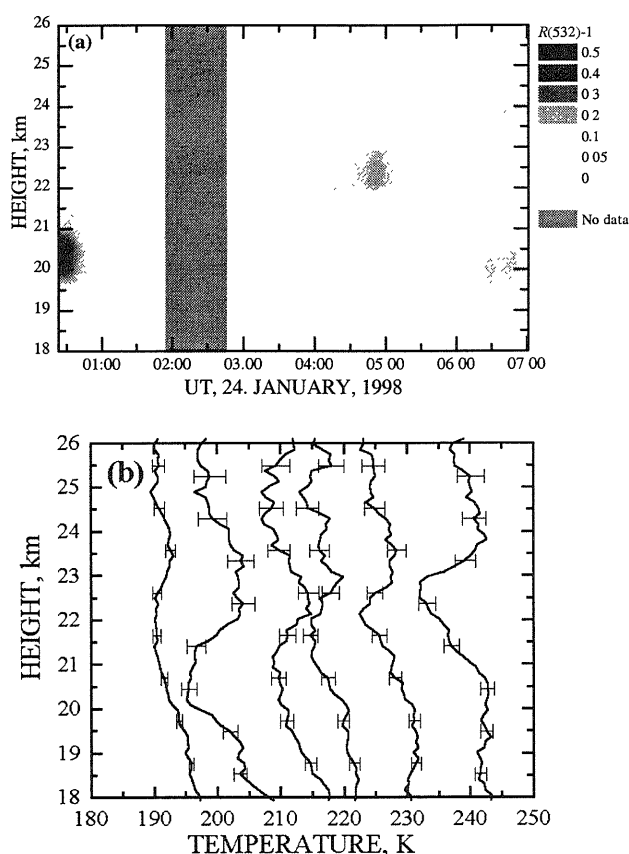

Figure 4. Temperature measurements in mountain-wave induced polar stratospheric clouds at Esrange on 24 January 1998: (a) Backscatter ratio - 1 measured at 532.25 nm. The data were smoothed with a gliding average window of 960 m and 10 minutes. (b) Temperature profiles measured at 0:23-5:26 UT, 0:23-1:03 UT, 1:03-1:56 UT, 2:53-3:49 UT, 3:49-4:46 UT, and 4:46-5:26 UT with 10 K offset between consecutive profiles. The data were smoothed with a gliding average window of 960 m.

stable. Multi-cavity interference filters made it possible to extract rotational Raman lines with pronounced temperature dependence. No sign of particle backscatter influence on the derived temperature profiles was detected. Temperature profiles with unprecedented spatial and temporal resolution have been measured up to 40 km height.

References

Y. F. Arshinov, S. M. Bobrovnikov, V. E. Zuev, V. M. Mitev (1983). Atmospheric temperature measurements using a pure rotational Raman lidar, Appl. Opt. **22**, 2984-2990.

A. Behrendt, J. Reichardt, C. Weitkamp, B. Neidhart (1998). Sequential tilted interference filter polychromator as a lidar receiver for rotational Raman temperature measurements in the troposphere and stratosphere, In: U.N. Singh et al. (Ed.), Proceedings of the 19th International Laser Radar Conference, Annapolis, Maryland, USA, 6 - 10 July 1998, NASA/CP-1998-207671/PT2, 641-634.

A. Behrendt, J. Reichardt, C. Weitkamp (1999). Temperature profiles from rotational Raman lidar: parameter for the interpretation of PSC composition, Proceedings of Workshop on Mesoscale Processes in the Stratosphere, Bad Tölz, Germany, 9 - 11 November 1998.

A. Behrendt and J. Reichardt (1999). Tunable sequential interference filter polychromator for rotational Raman temperature measurements, Appl. Opt., submitted.

J. Cooney (1972). Measurement of atmospheric temperature profiles by Raman backscatter, Appl. Meteor. **11**, 108-112.

P. Keckhut, M.L. Chanin, A. Hauchecorne (1990). Stratosphere temperature measurement using Raman lidar, Appl. Opt. **29**, 5182-5186.

T. Kitada, A. Hori, T. Taira, and T. Kobayashi (1994). Strange behaviour of the measurement of atmospheric temperature profiles of the rotational Raman lidar, Proceedings of the 17th International Laser Radar Conference, Sendai, Japan, 25 - 29 July 1994, 567-568.

D. Nedeljkovic, A. Hauchecorne, M. L. Chanin (1993). Rotational Raman lidar to measure the atmospheric temperature from the ground to 30 km, IEEE Trans. Geo. Rem. Sens. **31**, 90-101.

J. Reichardt, U. Wandinger, M. Serwazı, C. Weitkamp (1996). Combined Raman lidar for aerosol, ozone, and moisture measurements, Opt. Eng. **35**, 1457-1465.

G. Vaughan, D. P. Wareing, S. J. Pepler, L. Thomas, V. Mitev (1993). Atmospheric temperature measurements made by rotational Raman scattering, Appl. Opt. **32**, 2758-2764.

C. Weitkamp, J. Reichardt, A. Behrendt, A. Ansmann, M. Riebesell, U. Wandinger, (1999). Capabilities of a multipurpose Raman lidar, this Symposium.